Electronic structure, spin excitations, and orbital ordering in a three-orbital model for iron pnictides.

Sayandip Ghosh* and Avinash Singh Department of Physics, Indian Institute of Technology Kanpur 208016, India

A three-orbital itinerant-electron model involving d_{xz} , d_{yz} and d_{xy} Fe 3d orbitals is proposed for iron pnictides towards understanding the $(\pi,0)$ ordered magnetism and magnetic excitations in these materials. It is shown that this model simultaneously reproduces several experimentally observed features such as circular hole and elliptical electron pockets in the electronic Fermi surface structure, quantitatively correct spin wave dispersion, as well as the ferro orbital order between the d_{xz} and d_{yz} orbitals.

PACS numbers: 74.70.Xa, 75.10.Lp, 75.30.Ds, 75.25.Dk

I. INTRODUCTION

Iron pnictides exhibit a rich temperature-doping phase diagram^{1,2} involving antiferromagnetic (AF), structural and superconducting phase transitions. Several important microscopic properties such as electronic Fermi surface structure, orbital order and spin wave excitations have been extensively investigated experimentally using angle resolved photoemission spectroscopy (ARPES), x-ray linear dichroism (XLD), and neutron scattering. From a theoretical point of view, multi-orbital nature of these materials makes it challenging to understand these properties within a single theoretical framework.

First principle band-structure calculations^{3–5} have suggested that the density of states (DOS) near Fermi energy is contributed primarily by Fe 3d-bands.^{4,5} These calculations and ARPES experiments^{6–10} have revealed that there are two circular hole pockets around the center (Γ point) and two elliptical electron pockets around the corner (M point) of the 2D Brillouin Zone (BZ) in the paramagnetic state. The Fermi surface (FS) goes through a complex multi-orbital reconstruction through the paramagnetic-to-antiferromagnetic transition.^{6,8} Apart from the FS structure, ARPES^{8,11,12} and XLD^{13} experiments have also revealed the existence of ferro orbital order between d_{xz} and d_{yz} Fe orbitals. In the magnetic state, the Fe d_{yz} band is shifted up relative to the d_{xz} band, causing electron density difference between the two orbitals, which may cause structural phase transition. 14

In addition to electronic and structural properties, single crystal neutron scattering experiments have revealed a stripe antiferromagnetic arrangement of Fe moments in pnictides, corresponding to an in-plane ordering wave vector $\mathbf{Q} = (\pi, 0)$. Experimental investigation of spin wave excitations in these materials has been extensively carried out by inelastic neutron scattering (INS) measurements, ^{15–20} and the most striking feature is the remarkably high energy scale of magnetic excitations. The spin wave excitations are sharp, highly dispersive, and extend up to energies of ~ 200 meV with a well-defined maximum at the ferromagnetic zone boundary (FZB) corresponding to wave vector $\mathbf{q} = (\pi, \pi)$.

The observed spin wave excitations have strong in-plane anisotropy, with moderate¹⁷ to large damping,²⁰ but the excitations do not dissolve into particle hole continuum.¹⁶

Understanding all these magnetic, electronic, and structural properties exhibited by iron pnictides using a single theoretical framework continues to be an outstanding challenge. Although several tight-binding models have been proposed to address these properties, they tend to properly describe either the electronic or the magnetic properties, but not simultaneously both. For example, single band t - t' Hubbard model²¹ gives stable $(\pi,0)$ state at intermediate hole doping with carrierinduced ferromagnetic (F) spin couplings, correct spin wave dispersion, but does not yield the correct electronic structure. Among the two-orbital models, ^{22–24} the minimal two-band model by Raghu et al.²² reproduces the FS structure consistent with LDA calculations at half-filling, and nesting between circular hole and electron pockets significantly reduces the critical interaction strength U_c for $(\pi,0)$ ordering. However, spin wave dispersion in this model does not agree in detail with INS measurements. 25,26 Moreover, it does not include d_{xy} Fe orbital which contributes some portions of the electron pockets. Similarly, three-orbital models with one-third filling (i.e. two electrons in three orbitals),²⁷ two-third filling (i.e. four electrons in three orbitals), 28,29 and fourorbital model at half-filling³⁰ can reproduce the desired FS structure, but spin wave excitations in these models have not been investigated yet. More realistic fiveorbital models^{31–33} were proposed aimed at the investigation of pairing instabilities. While these models vield the FS topology similar to experimental findings, they do not account for observed spin wave dispersion. Although anisotropic spin wave excitation was obtained in a recent study³⁴ for a five-orbital model,³⁵ the electron pockets obtained in this model are not elliptical and there is an additional spurious d_{xy} dominated hole pocket, contrary to ARPES experiments. Moreover, investigation of spin excitations over the entire BZ was not carried out.

In this context, we present and investigate a threeorbital itinerant-electron model in this paper. We find that this minimal model simultaneously yields the correct FS topology as well as spin wave dispersion consistent

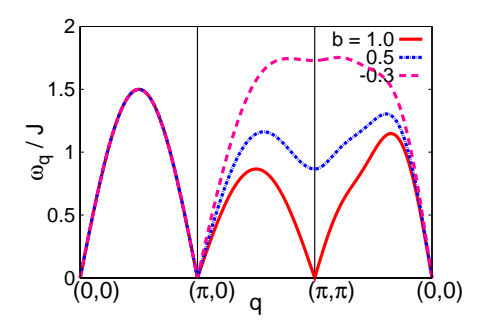


FIG. 1: Spin wave dispersion along different BZ directions obtained from Eq. [1] for J'/J=1 and different values of the coefficient b corresponding to different F spin couplings — (i) b=1 (no F spin coupling), (ii) b=0.5 (intermediate case), and (iii) b<0 ($J_{\rm F}>J_{\rm AF}$), which yields maximum spin wave energy at the ferromagnetic zone boundary (π,π) .

with INS experiments. Moreover, ferro orbital order of appropriate sign is also obtained in this model.

The organization of this paper is as follows. The importance of ferromagnetic (F) spin couplings on the experimentally measured spin wave dispersion in the $(\pi,0)$ state is briefly discussed in section II. Then in section III, it is shown that no F spin coupling is generated in the two-band model with FS nesting, ²² although this model yields correct FS topology. A third d_{xy} Fe orbital is therefore necessary to overcome this shortcoming, and a three-orbital model having d_{xz} , d_{yz} and d_{xy} Fe 3d orbitals is presented in section IV highlighting the Fermi surface and density of states. The investigation of magnetic excitations and orbital ordering in the $(\pi,0)$ magnetic state is carried out in section V and section VI, respectively. Finally conclusions are presented in section VII.

II. SPIN WAVE ENERGY AT THE FERROMAGNETIC ZONE BOUNDARY AND FERROMAGNETIC SPIN COUPLING

In order to highlight the effect of induced F spin couplings on the spin wave dispersion and spin wave energy at the FZB, we consider the case of single band Hubbard model with nearest-neighbor (NN) hopping t and next-nearest-neighbor (NNN) hopping t'. In this case, the spin wave dispersion in the strong coupling limit³⁶ is given by,

$$\left(\frac{\omega_{\mathbf{q}}}{J}\right)^{2} = \left\{ \left(1 + \frac{2J'}{J}\right) - b(1 - \cos q_{y}) \right\}^{2}$$
$$-\left\{ \left(1 + \frac{2J'}{J}\cos q_{y}\right)\cos q_{x} \right\}^{2}. \tag{1}$$

where $J=4t^2/U$ and $J'=4t'^2/U$ represent the NN and NNN AF spin couplings respectively, and the coefficient b=1 at half-filling. In presence of doping, carrier-induced F spin coupling are generated,²¹ and the spin wave dispersion can be well described by the same expression where, $b \sim (J_{\rm AF}-J_{\rm F})/J_{\rm AF}$ provides a relative

measure of the F and AF spin coupling strengths. The case b=1 corresponds to zero F spin couplings, as obtained for the half-filled t-t' Hubbard model, and yields zero spin wave energy $(\omega_{\rm FZB})$ at the zone boundary in the ferromagnetic direction (π,π) . With the onset of F spin couplings (b<1) as in the doped t-t' Hubbard model, 21 the spin wave energy at this wave vector increases from zero [Fig. 1]. When the coefficient b becomes negative at sufficiently large F spin couplings, the spin wave energy at this wave vector becomes maximum over the entire Brillouin zone, as indeed is observed in INS measurements on iron pnictides.

III. ABSENCE OF FERROMAGNETIC SPIN COUPLING IN THE TWO-BAND NESTING MODEL

We will now investigate spin wave excitations in the minimal two-band model²² which has been investigated intensively in recent years. The model has two degenerate d_{xz} and d_{yz} orbitals in 2D, and yields nearly circular hole pockets at (0,0), $(\pm \pi, \pm \pi)$ and electron pockets at $(\pm \pi,0)$, $(0,\pm \pi)$. The appreciable FS nesting results in strong instability towards $(\pi,0)$ or $(0,\pi)$ magnetic ordering at significantly low values of the interaction strength $(U_c \approx 3)$. However, as we will see in this section, the very same critical features for FS nesting (nearly identical circular hole and electron pockets) also necessarily imply vanishing F spin couplings and consequent vanishing of $\omega_{\rm FZB}$, in sharp contrast with INS measurements.

The tight-binding part of the Hamiltonian is defined as

$$H_0 = -\sum_{\mathbf{i},\mathbf{j}} \sum_{\mu,\nu} \sum_{\sigma} t_{\mathbf{i},\mathbf{j}}^{\mu,\nu} (a_{\mathbf{i},\mu,\sigma}^{\dagger} a_{\mathbf{j},\nu,\sigma} + \text{H.c.}), \qquad (2)$$

where \mathbf{i}, \mathbf{j} refer to site indices, μ, ν are the orbital indices, and $t_{\mathbf{i}, \mathbf{i}}^{\mu, \nu}$ are the hopping terms as defined as Ref. 22.

Figure 2 shows the Fermi surface structure for this model. The hopping parameters are t_1 =-1.0, t_2 =1.3, t_3 = t_4 =-0.85, and Fermi energy E_F =1.45, in units of $|t_1|$. This Fermi energy corresponds to total electron filling $n \approx 2.0$. In the large BZ (for 1 Fe/cell) [Fig. 2(a)], there are two hole pockets and two electron pockets. After folding along the faint line in Fig. 2(a), FS topology in the actual crystallographic BZ is obtained as in Fig. 2(b), which is similar to LDA calculations.

The interaction Hamiltonian consists of different onsite electron-electron interactions:

$$H_{I} = U \sum_{\mathbf{i},\mu} n_{\mathbf{i},\mu,\uparrow} n_{\mathbf{i},\mu,\downarrow} + (U' - \frac{J}{2}) \sum_{\mathbf{i},\mu,\nu}^{\mu<\nu} n_{\mathbf{i},\mu} n_{\mathbf{i},\nu}$$

$$- 2J \sum_{\mathbf{i},\mu,\nu}^{\mu<\nu} \mathbf{S}_{\mathbf{i},\mu} \cdot \mathbf{S}_{\mathbf{i},\nu}$$

$$+ J' \sum_{\mathbf{i},\mu,\nu}^{\mu<\nu} (a_{\mathbf{i},\mu,\uparrow}^{\dagger} a_{\mathbf{i},\mu,\downarrow}^{\dagger} a_{\mathbf{i},\nu,\downarrow} a_{\mathbf{i},\nu,\uparrow} + \text{H.c.}), \qquad (3)$$

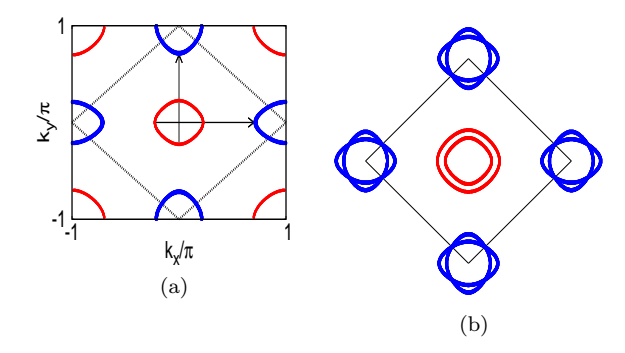


FIG. 2: Fermi surface for the two band model with $t_1 = -1.0$, $t_2 = 1.3$, $t_3 = t_4 = -0.85$ in the (a) unfolded (1 Fe atom/unit cell) BZ and (b) folded BZ. The hole and electron pockets are separated by wave-vector $(\pi, 0)$ and $(0, \pi)$, showing Fermi surface nesting. The Fermi energy $E_F = 1.45|t_1|$ for $n \approx 2.0$.

where $\mathbf{S}_{i,\mu}$ $(n_{\mathbf{i},\mu})$ refer to the local spin (charge) density operators. The first and second terms are the intra-orbital and inter-orbital Coulomb interactions respectively, the third term is the Hund's coupling and the fourth term the "pair-hopping" term whose coupling strength J' is equal to J. From rotational symmetry, U' = U - 2J.

The static susceptibility in the paramagnetic state has strong enhancements at $(\pm \pi, 0)$, $(0, \pm \pi)$ due to nesting between hole and electron Fermi pockets, ^{22,37} favoring transition to a $(\pi, 0)$ ordered spin density wave (SDW) state at some low critical interaction strength.

In the $(\pi,0)$ state, the Hartree-Fock level (mean-field) Hamiltonian matrix in the composite sublattice-orbital basis (Axz Ayz Bxz Byz) takes the form:

$$H_{\mathrm{HF}}^{\sigma}(\mathbf{k}) = \begin{bmatrix} -\sigma \Delta_{xz} + \varepsilon_{\mathbf{k}}^{2y} & 0 & \varepsilon_{\mathbf{k}}^{1x} + \varepsilon_{\mathbf{k}}^{3} & \varepsilon_{\mathbf{k}}^{4} \\ 0 & -\sigma \Delta_{yz} + \varepsilon_{\mathbf{k}}^{1y} & \varepsilon_{\mathbf{k}}^{4} & \varepsilon_{\mathbf{k}}^{2x} + \varepsilon_{\mathbf{k}}^{3} \\ \varepsilon_{\mathbf{k}}^{1x} + \varepsilon_{\mathbf{k}}^{3} & \varepsilon_{\mathbf{k}}^{4} & \sigma \Delta_{xz} + \varepsilon_{\mathbf{k}}^{2y} & 0 \\ \varepsilon_{\mathbf{k}}^{4} & \varepsilon_{\mathbf{k}}^{2x} + \varepsilon_{\mathbf{k}}^{3} & 0 & \sigma \Delta_{yz} + \varepsilon_{\mathbf{k}}^{1y} \end{bmatrix}$$

for spin $\sigma = +(-)$ for spin $\uparrow(\downarrow)$, where the band energies

$$\epsilon_{\mathbf{k}}^{1x} = -2t_1 \cos k_x, \qquad \epsilon_{\mathbf{k}}^{2x} = -2t_2 \cos k_x,
\epsilon_{\mathbf{k}}^{1y} = -2t_1 \cos k_y, \qquad \epsilon_{\mathbf{k}}^{2y} = -2t_2 \cos k_y,
\epsilon_{\mathbf{k}}^{3} = -4t_3 \cos k_x \cos k_y, \qquad \epsilon_{\mathbf{k}}^{4} = -4t_4 \sin k_x \sin k_y,$$
(5)

corresponding to different hopping terms in different directions, and the self-consistently determined exchange fields:

$$2\Delta_{xz} = Um_{xz} + Jm_{yz}$$

$$2\Delta_{yz} = Um_{yz} + Jm_{xz}$$
(6)

in terms of the sublattice magnetizations m_{xz} and m_{yz} for the two orbitals. For a given Fermi energy E_F ,

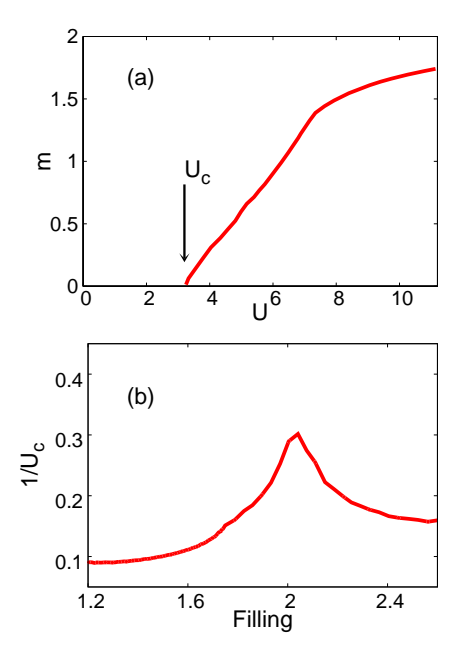


FIG. 3: (a) Variation of sublattice magnetization with U for $n \approx 2.0$ and $J{=}0$, showing onset of $(\pi,0)$ magnetic order at critical interaction strength $U_c \approx 3.0$. (b) The inverse of critical interaction U_c^{-1} shows a maximum around electron filling $n \approx 2.0$ corresponding to nesting between hole and electron Fermi pockets, showing proclivity of the two-band system towards $(\pi,0)$ magnetic ordering.

the sublattice magnetization is obtained from the corresponding electronic densities as

$$m_{\mu} = n_{\uparrow}^{\mu A} - n_{\downarrow}^{\mu A} = n_{\downarrow}^{\mu B} - n_{\uparrow}^{\mu B} = n_{\uparrow}^{\mu A} - n_{\uparrow}^{\mu B}$$
$$= \sum_{\mathbf{k},l} [(\phi_{\mathbf{k},\uparrow,l}^{\mu,A})^{2} - (\phi_{\mathbf{k},\uparrow,l}^{\mu,B})^{2}] \Theta(E_{F} - E_{\mathbf{k},\uparrow,l}). \quad (7)$$

Here $E_{\mathbf{k},\sigma,l}$ and $\phi_{\mathbf{k},\sigma,l}$ are the eigenvalues and eigenvectors of the Hamiltonian matrix (Eqn. 4), where the index l refers to the four eigenvalue branches. The pair hopping term does not contribute to the mean field Hamiltonian (4) in the magnetic state.

Figure 3(a) shows the evolution of the total sublattice magnetization $m=m_{xz}+m_{yz}$ at half-filling with interaction U. Onset of magnetization at $U\approx 3.0$ indicates the magnetic instability of the system at the critical interaction $U_c\approx 3.0$. Variation of U_c with electron filling [Fig. 3(b)] shows that U_c for $(\pi,0)$ ordering has lowest value at half-filling for which the electron and hole pockets are well nested. This highlights the proclivity of the two-band system towards $(\pi,0)$ ordering due to FS nesting.

Using eigenvalues and eigenvectors of the Hartree-Fock (HF) level Hamiltonian in the $(\pi,0)$ state, we have calculated the spin wave energies, as described in the Appendix A. The calculated spin wave energies along various symmetry directions of the BZ are shown in Fig. 4. The AF ordering is stable with positive spin wave energies along AF direction, but spin wave energy at

the zone boundary in the ferromagnetic direction vanishes, which is in sharp contrast to the maximum spin wave energy observed at this wave vector in INS experiments (dotted line). Thus, while the two band model with circular pockets exhibits high magnetic susceptibility at $n \approx 2.0$, it does not yield a stable $(\pi, 0)$ magnetic state with strong ferromagnetic spin couplings as indicated by INS experiments. The reason for this dichotomy is as below. Maximum spin wave energy at the FZB requires strong ferromagnetic spin couplings as discussed in Sec. II. According to band theory of ferro magnetism, the induced F spin coupling is determined by $\langle \nabla^2_{\mathbf{k}} E_{\mathbf{k}} \rangle$ which involves the electron band curvature. Nearly identical circular hole and electron pockets yield ferromagnetic spin coupling contributions of similar magnitude but opposite sign, resulting in cancellation and hence no net F spin coupling is induced.

While the strong magnetic response of a system with Fermi surface nesting towards $(\pi, 0)$ magnetic ordering may suggest presence of both AF and F spin couplings in respective directions, that is actually not the case. Indeed, the $(\pi,0)$ state can be stabilized by only AF spin couplings, as realized in the half-filled t-t' Hubbard model for t' > t/2 in two dimensions.³⁶ While the nearest-neighbor (NN) AF spin couplings get fully frustrated in this magnetic state, the next-nearest-neighbor (NNN) AF spin couplings stabilize the $(\pi, 0)$ state which involves AF spin ordering in the diagonal (NNN) directions. That the spin wave dispersion obtained for the two-band model with Fermi-surface nesting [Fig. 4] is similar to that of the half-filled t - t' Hubbard model [Fig. 1] clearly shows that the $(\pi,0)$ magnetic state in the two-band model is stabilized by only AF spin couplings. Thus, we infer that although nesting condition of the two-band model at total electron filling $n \approx 2.0$ strongly enhances the proclivity of the system towards $(\pi,0)$ magnetic ordering, it results in identically vanishing F spin coupling. Hence, a third d_{xy} orbital must be included with appropriate electron filling to ensure sufficiently strong F spin coupling so as to obtain maximum spin wave energy at the FZB as observed in INS experiments.

IV. THREE-ORBITAL MODEL

As explained in the previous section, in order to account for the spin wave excitations in iron pnictides, the minimal multi-orbital model should consist of three orbitals. We therefore consider a three-orbital model in which a third d_{xy} orbital is included with appropriate electron filling, and the d_{xz} and d_{yz} orbitals of the two-band model are retained with electron filling in these orbitals correspondingly reduced to maintain total electron filling $n \approx 2$.

All iron prictides have quasi-two dimensional crystal structure with layers of FeAs stacked along the c axis. The As ions sit alternately above and below the square

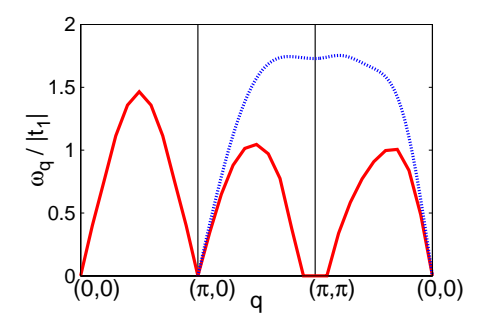


FIG. 4: The spin wave dispersion (red solid line) for the two-band model with Fermi surface nesting (total electron filling $n \approx 2.0$) shows identical behavior as for the half-filled t-t' Hubbard model [Fig. 1]. The spin wave energy at the ferromagnetic direction zone boundary (π,π) vanishes, whereas typical INS measurements on iron pnictides show a maximum at this wave vector (blue dotted line). Here, $\Delta_{xz} = \Delta_{yz} = 2.0 |t_1|$ for $U \approx 5.0 |t_1|$ and $J \approx U/4$.

plaquettes formed by Fe ions and all interesting phenomena of superconductivity and magnetism originate from these FeAs layers. We focus on these FeAs planes and construct a 2D three-orbital model of Fe d_{xz} , d_{yz} and d_{xy} orbitals since these orbitals contribute to the bands near the Fermi energy.^{8,38,39} The orbitals are labeled as xz, yz, and xy respectively. Hybridization of Fe 3d orbitals with themselves and through As 3p orbitals contribute to the effective Fe-Fe hoppings in our model. While xz and yz are degenerate due to C_4 symmetry, xy has a higher onsite energy due to crystal field splitting.

Before we proceed further, one important issue that needs to be clarified is the electron filling in the threeorbital model. In prictides, each iron ion has six electrons distributed among five Fe 3d orbitals. Band structure calculations show that the two e_g orbitals $d_{3z^2-r^2}$ and $d_{x^2-y^2}$ are completely occupied by four electrons due to large crystal field splitting between t_{2g} and e_g states. Therefore, the total electron filling in our three-orbital model will be one-third (i.e. two electrons in three orbitals). Due to this one-third filling, 28 we obtain hole pockets around Γ and M points of extended BZ. Other three-orbital models^{28,29} have obtained two hole pockets around Γ points, but electron filling in those models is two-third (i.e. four electrons in three orbitals). Due to alternate position of As atoms in FeAs planes, the actual crystallographic unit cell has $\sqrt{2} \times \sqrt{2}$ structure with 2 Fe/cell and the corresponding BZ is folded. After folding, we obtain two hole pockets around the center of crystallographic BZ which is in agreement with the findings of ARPES experiments.

The tight binding Hamiltonian consists of hopping term and onsite energy term

$$H_{0} = -\sum_{\mathbf{i},\mathbf{j}} \sum_{\mu,\nu} \sum_{\sigma} t_{\mathbf{i},\mathbf{j}}^{\mu,\nu} (a_{\mathbf{i},\mu,\sigma}^{\dagger} a_{\mathbf{j},\nu,\sigma} + \text{H.c.}) + \sum_{\mathbf{i}} \sum_{\mu} \varepsilon_{\mu} n_{\mathbf{i},\mu},$$
(8)

where $a_{{\bf i},\mu,\sigma}^{\dagger}$ creates an electron at site ${\bf i}$ with spin σ in

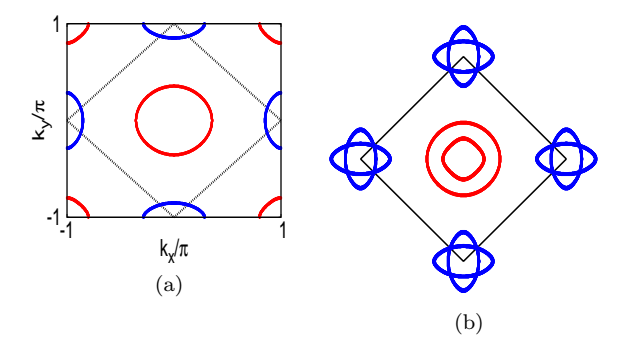


FIG. 5: Fermi surface in the three-orbital model with hopping parameters as given in Table I in the (a) unfolded (1 Fe/cell) BZ and (b) folded BZ. The two circular hole pockets (red) and elliptical electron pockets (blue) are in agreement with ARPES experiments.

TABLE I: Value of hopping parameters in the three-orbital model. All the hoppings are in units of $|t_1|$.

t_1	t_2	t_3	t_4	t_5	t_6	t_7	t_8
-1.0	0.5	-0.6	-0.6	-1.0	-0.6	0.3	0.15

the μ -th orbital, and $t_{\mathbf{i},\mathbf{j}}^{\mu,\nu}$ are the hopping amplitudes. We consider NN and NNN hoppings for all the orbitals. The hopping tensor $t_{\mathbf{i},\mathbf{j}}^{\mu,\nu}$ is defined in the same way as in Ref 28. ε_{μ} is the onsite energy for the μ -th orbital.

In the plane wave basis defined as $a_{\mathbf{i},\mu,\sigma} = \frac{1}{\sqrt{N}} \sum_{\mathbf{k}} e^{i\mathbf{k}\cdot\mathbf{r}_i} a_{\mathbf{k},\mu,\sigma}$, the tight-binding Hamiltonian is given by

$$H_0 = \sum_{\mathbf{k}} \sum_{\sigma} \sum_{\mu,\nu} T^{\mu,\nu}(\mathbf{k}) a^{\dagger}_{\mathbf{k},\mu,\sigma} a_{\mathbf{k},\nu,\sigma}, \tag{9}$$

where

$$T^{11} = -2t_1 \cos k_x - 2t_2 \cos k_y - 4t_3 \cos k_x \cos k_y$$

$$T^{22} = -2t_2 \cos k_x - 2t_1 \cos k_y - 4t_3 \cos k_x \cos k_y$$

$$T^{33} = -2t_5 (\cos k_x + \cos k_y) - 4t_6 \cos k_x \cos k_y$$

$$+ \varepsilon_{\text{diff}}$$

$$T^{12} = T^{21} = -4t_4 \sin k_x \sin k_y$$

$$T^{13} = \bar{T}^{31} = -2it_7 \sin k_x - 4it_8 \sin k_x \cos k_y$$

$$T^{23} = \bar{T}^{32} = -2it_7 \sin k_y - 4it_8 \sin k_y \cos k_x$$
 (10)

are the tight-binding matrix elements in the unfolded BZ $(-\pi \le k_x, k_y \le \pi)$. The crystallographic BZ is folded $(|k_x| + |k_y| \le \pi)$ and folding doubles the number of bands to six. Here, t_1 and t_2 are the intra-orbital hopping for xz (yz) along x(y) and y(x) directions respectively; t_3 is the intra-orbital hopping along diagonal direction for xz and yz; t_4 inter-orbital hopping between xz and yz; t_5 and t_6 are intra-orbital NN and NNN hoppings for xy; t_7 and t_8 the NN and NNN hybridization between xy and xz/yz. Finally, $\varepsilon_{\rm diff}$ is the energy difference between the xy and degenerate xz/yz orbitals.

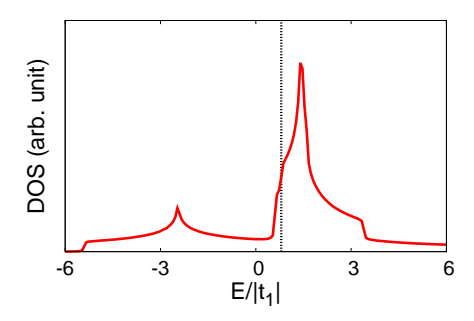


FIG. 6: The total density of states (DOS) in the three-orbital model showing two Van Hove singularities. The Fermi energy (dashed line) lies near the upper singularity corresponding to the quasi one-dimensional character of the d_{xy} band.

A. Fermi Surface

The Fermi surface for the three-orbital tight-binding Hamiltonian in Eq. 9 is shown in Fig 5 with the hopping parameter values as listed in Table I. This set of hopping parameters will be used throughout this work. Here, Fermi energy and energy difference for d_{xy} are chosen to be $E_F{=}0.8$ and $\varepsilon_{\mathrm{diff}}{=}3.2$ to ensure one-third electron filling. All the energies are in unit of $|t_1|$. As shown in Fig. 5(a), there are nearly circular hole pockets around the center (0,0) and the corners $(\pm \pi, \pm \pi)$ and elliptical electron pockets each around $(\pm \pi, 0)$ and $(0, \pm \pi)$ in the unfolded BZ. The faint line in Fig. 5(a) marks the crystallographic BZ corresponding to 2 Fe atoms per unit cell. Folding along the faint line yields two nearly circular hole pockets around the Γ point and two elliptical electron pockets around the M point [Fig. 5(b)] of the crystallographic BZ. Thus we see that our three-orbital model can reproduce the FS structure found out in LDA calculations and observed in ARPES experiments. Similar FS topology was also obtained in two-band model mentioned earlier. However, the electron pockets obtained were nearly circular in contrast to elliptical pockets observed in experiments.

B. Density of States

The density of states (DOS) for the three-orbital model is shown in Fig 6. It has two Van Hove singularities similar to LDA results and two-band model. However, in contrast to the two-band model where the Fermi energy lies in the flat region of the band, in our model it is in the vicinity of one of the Van Hove singularities. This singularity comes from the third band (highest in energy) which is primarily of d_{xy} character. Elliptical electron pocket corresponds to quasi-one dimensional character, which has a DOS peak near the lower band edge. Consequently, $\langle \nabla^2_{\bf k} E_{\bf k} \rangle$ is large which favors strong F spin coupling according to band theory of ferromagnetism. Thus, the ellipticity of electron Fermi pockets in our model plays a pivotal role in generating strong F

spin coupling and therefore maximum spin wave energy at (π, π) , as investigated in the following section.

V. MAGNETIC EXCITATIONS IN THE $(\pi, 0)$ SDW STATE

In this section we will study magnetic excitations in the $(\pi, 0)$ magnetic state in the three-orbital model in-

troduced in the last section. We will include various electron-electron interaction terms as described in Eq. 3. As the intermediate-coupling regime will be considered throughout, the term SDW state is used here without any implicit weak-coupling connotation.

Performing Hartree-Fock approximation as described in Appendix B, HF level (mean-field) Hamiltonian matrix in this composite sublattice-orbital basis (Axz Ayz Axy Bxz Byz Bxy) is obtained as:

$$H_{\mathrm{HF}}^{\sigma}(\mathbf{k}) = \begin{bmatrix} -\sigma \Delta_{xz} + \varepsilon_{\mathbf{k}}^{2y} & 0 & 0 & \varepsilon_{\mathbf{k}}^{1x} + \varepsilon_{\mathbf{k}}^{3} & \varepsilon_{\mathbf{k}}^{4} & \varepsilon_{\mathbf{k}}^{7x} + \varepsilon_{\mathbf{k}}^{8,1} \\ 0 & -\sigma \Delta_{yz} + \varepsilon_{\mathbf{k}}^{1y} & \varepsilon_{\mathbf{k}}^{7y} & \varepsilon_{\mathbf{k}}^{4} & \varepsilon_{\mathbf{k}}^{2x} + \varepsilon_{\mathbf{k}}^{3} & \varepsilon_{\mathbf{k}}^{8,2} \\ 0 & -\varepsilon_{\mathbf{k}}^{7y} & -\sigma \Delta_{xy} + \varepsilon_{\mathbf{k}}^{5y} + \tilde{\varepsilon}_{\mathrm{diff}} & -\varepsilon_{\mathbf{k}}^{7x} - \varepsilon_{\mathbf{k}}^{8,1} & -\varepsilon_{\mathbf{k}}^{8,2} & \varepsilon_{\mathbf{k}}^{5x} + \varepsilon_{\mathbf{k}}^{6} \\ \varepsilon_{\mathbf{k}}^{1x} + \varepsilon_{\mathbf{k}}^{3} & \varepsilon_{\mathbf{k}}^{4} & \varepsilon_{\mathbf{k}}^{7x} + \varepsilon_{\mathbf{k}}^{8,1} & \sigma \Delta_{xz} + \varepsilon_{\mathbf{k}}^{2y} & 0 & 0 \\ \varepsilon_{\mathbf{k}}^{4} & \varepsilon_{\mathbf{k}}^{2x} + \varepsilon_{\mathbf{k}}^{3} & \varepsilon_{\mathbf{k}}^{8,2} & \sigma \Delta_{xz} + \varepsilon_{\mathbf{k}}^{2y} & 0 & 0 \\ -\varepsilon_{\mathbf{k}}^{7x} - \varepsilon_{\mathbf{k}}^{8,1} & -\varepsilon_{\mathbf{k}}^{8x} & \varepsilon_{\mathbf{k}}^{8x} & 0 & \sigma \Delta_{yz} + \varepsilon_{\mathbf{k}}^{1y} & \varepsilon_{\mathbf{k}}^{7y} \\ -\varepsilon_{\mathbf{k}}^{7x} - \varepsilon_{\mathbf{k}}^{8,1} & -\varepsilon_{\mathbf{k}}^{8x} & \varepsilon_{\mathbf{k}}^{5x} + \varepsilon_{\mathbf{k}}^{6} & 0 & -\varepsilon_{\mathbf{k}}^{7y} & \sigma \Delta_{xy} + \varepsilon_{\mathbf{k}}^{5y} + \tilde{\varepsilon}_{\mathrm{diff}} \end{bmatrix}$$

$$(11)$$

for spin σ , where

$$\varepsilon_{\mathbf{k}}^{1x} = -2t_1 \cos k_x \qquad \varepsilon_{\mathbf{k}}^{1y} = -2t_1 \cos k_y
\varepsilon_{\mathbf{k}}^{2x} = -2t_2 \cos k_x \qquad \varepsilon_{\mathbf{k}}^{2y} = -2t_2 \cos k_y
\varepsilon_{\mathbf{k}}^{5x} = -2t_5 \cos k_y \qquad \varepsilon_{\mathbf{k}}^{5y} = -2t_5 \cos k_y
\varepsilon_{\mathbf{k}}^{3} = -4t_3 \cos k_x \cos k_y \qquad \varepsilon_{\mathbf{k}}^{4} = -4t_4 \sin k_x \sin k_y
\varepsilon_{\mathbf{k}}^{6} = -4t_6 \cos k_x \cos k_y
\varepsilon_{\mathbf{k}}^{7y} = -2it_7 \cos k_x \qquad \varepsilon_{\mathbf{k}}^{7y} = -2it_7 \cos k_y
\varepsilon_{\mathbf{k}}^{8,1} = -4it_8 \sin k_x \cos k_y \qquad \varepsilon_{\mathbf{k}}^{8,2} = -4it_8 \cos k_x \sin k_y
(12)$$

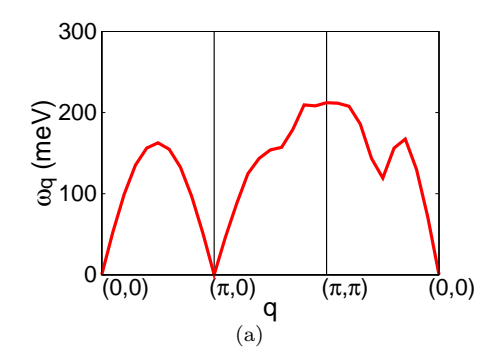
are the band energies corresponding to different hopping terms along different directions, and the self-consistent exchange fields are defined as $2\Delta_{\mu} = U m_{\mu} + J \sum_{\nu \neq \mu} m_{\nu}$ in terms of sublattice magnetizations m_{μ} obtained from the corresponding electronic densities as given in Eq. 7.

It should be noted that, apart from a constant term, the density term $(5J-U)n_{\mu}/2$ (for orbital μ) arising in the HF approximation has not been shown explicitly in Eqn. 11. Although the magnitude of this term can be appreciable, only the relative energy shifts $(5J-U)(n_{\mu}-n_{\nu})/2$ are important at fixed filling. For our choice of parameters, the shift between d_{xz} and d_{yz} orbital is very small ($\sim 0.03~U$), and is neglected in our calculations. Although the shift between d_{xy} and $d_{xz/yz}$ orbitals is appreciable, it has been absorbed in the renormalized energy difference $\tilde{\varepsilon}_{\rm diff}$ which has two components – (i) the orbital energy difference $\varepsilon_{\rm diff}$, and (ii) the relative energy shift due to density term in the HF approximation.

Spin-wave energies in this spontaneously brokensymmetry SDW state are calculated as described in the Appendix A. Negative spin wave energies are taken as signature of instabilities of the SDW state. INS experiments measure the dynamical spin structure factor $S(\mathbf{Q},\omega)$ which is proportional to the imaginary part of the transverse spin susceptibility. The transverse susceptibility is calculated by taking trace of the susceptibility matrix [Eq. A3]. All our calculations are done at zero temperature.

Figure 7(a) shows the spin wave energy dispersion along the path $(0,0)\rightarrow(\pi,0)\rightarrow(\pi,\pi)\rightarrow(0,0)$ of the unfolded BZ. For $U \approx 5.0$, $J \approx U/4$ and total filling $n \approx 2.0$, the self-consistent exchange fields are $\Delta_{xz} \approx 2.4$, $\Delta_{yz} \approx 1.9$, and $\Delta_{xy} \approx 1.4$. The Fermi energy (E_F) and renormalized energy difference ($\tilde{\varepsilon}_{\text{diff}}$) values are -1.15and 1.7 respectively. All the energies are in units of $|t_1|$. We see that that not only is the $(\pi, 0)$ SDW state stable throughout the BZ in our model, strong ferromagnetic spin coupling is also generated, as inferred from the maximum spin wave energy at FZB, which agrees well with the spin wave dispersion in INS experiments. For a realistic NN hopping value of $|t_1| \sim 200$ meV, the calculated maximum spin wave energy is $\sim 200 \text{ meV}$ which matches well with INS experiments. The interaction strength values $U \sim 1$ eV and $J \sim 0.25$ eV are also realistic and obey the constraints imposed by ARPES and INS experiments on coupling strength for iron pnictides.⁴⁰

The maximum spin wave energy at the FZB implies strong F spin coupling and $(\pi,0)$ SDW state is stabilized without any frustrating NN AF coupling. The $(\pi,0)$ state has been shown to be stable also within a spin-only Heisenberg model with comparable NN (J_1) and NNN (J_2) antiferromagnetic superexchanges.⁴¹ But such a model is strongly frustrated and can not explain the observed maximum of spin wave dispersion at (π,π) . In fact, it was shown that spin wave dispersion throughout the BZ and the maximum at (π,π) can be explained by



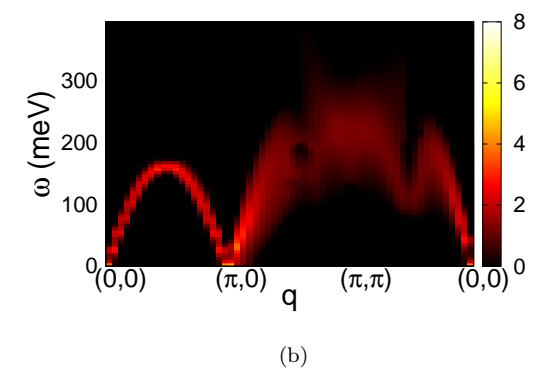


FIG. 7: (a) Spin wave dispersion in the $(\pi, 0)$ SDW state of the three-orbital model with hopping parameters as given in Table I and with $|t_1|$ =200 meV. The maximum energy around (π, π) is consistent with INS experiments. (b) Imaginary part of the transverse susceptibility for same parameters.

a suitably parameterized Heisenberg Hamiltonian with an effective ferromagnetic exchange interaction $(J_{1b} < 0)$ along b direction.¹⁷ The present work provides the microscopic origin of this ferromagnetic interaction as due to usual particle-hole exchange mediated spin interaction in an itinerant-electron model, with emergence of strong F spin coupling originating from elliptical nature of electron pockets reflecting quasi-one dimensional electron band.

Figure 7(b) shows the imaginary part of the transverse spin susceptibility, Im $[\chi_{\text{RPA}}^{-+}(\mathbf{q},\omega)]$ along the same path as in figure 7(a) for $|t_1| = 200$ meV. The intensity is shown on a log scale. The exchange fields and interaction values are same as in Fig. 7(a). Evidently, the spin wave excitations are highly dispersive with a strong in-plane anisotropy between AF $[(0,0) \rightarrow (\pi,0)]$ and F directions $[(\pi,0) \to (\pi,\pi)]$. The peak position of magnetic spectrum moves to higher energy along both paths, but fades away quickly along F direction, implying higher damping. However, we note that despite spin waves being damped at high energies along F direction, they form a closed structure over the entire BZ. Thus, in contrast to other itinerant models, ^{26,42} the magnetic excitations in our model do not rapidly dissolve into particle-hole continuum, as indeed not observed in experiments up to energies $\sim 200 \text{ meV}$.

The magnetic excitation spectrum in our model sat-

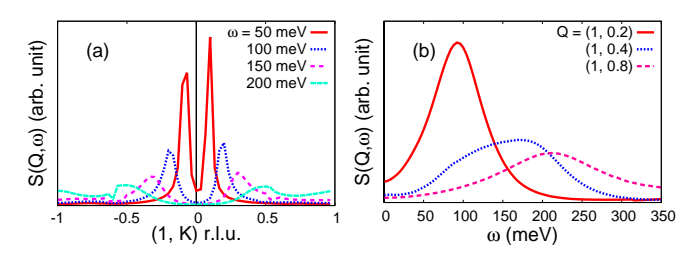


FIG. 8: (a) Constant-energy cuts along (1, K) direction at different energies, (b) Constant- \mathbf{Q} cuts of magnetic excitations for different \mathbf{Q} along F directions for same parameters as in Fig. 7(a) for $|t_1| = 200$ meV.

isfies Goldstone mode condition due to spin rotational invariance of the model Hamiltonian and yields zero spin wave energy at $\mathbf{q} = (0,0)$ and $(\pi,0)$. In the low temperature phase for iron pnictides, Fe moments allign along a direction suggesting the need to include single-ion magnetic anisotropy in our model. In fact, orthorhombic distortion can introduce such anisotropy through magnetoelastic coupling and break the rotational invariance. The resulting excitation spectrum will have a spin wave gap as measured in experiments. ^{15,16} However, the magnitude of the measured gap was found to be much smaller ($\leq 10 \text{ meV}$) than typical spin wave energy scale and can be neglected.

The scattering cross section in INS experiments is proportional to the dynamical structure factor $S(\mathbf{Q}, \omega)$ calculated from the imaginary part of the transverse susceptibility. Here, the wave vector \mathbf{Q} is defined as (H, K)in reciprocal lattice unit (r.l.u.). Figure 8(a) shows the constant energy cuts of $S(\mathbf{Q}, \omega)$ along the K direction from (1, 1) to (1, -1). At low energies, there are two peaks near (1,0). As the excitation energy increases, well-defined counter propagating spin waves approach the zone boundary. With increasing energy, the peak not only move towards zone boundary, its intensity is also reduced considerably. The position of the peaks and their energy dependence is in qualatative agreement with experimental results. ^{17,20} Fig. 8(b) shows the constant **Q**cuts of $S(\mathbf{Q}, \omega)$ for different \mathbf{Q} along F directions. Thus, well defined spin-wave excitations with increasing energy are obtained as **Q** approaches (1, 1) r.l.u. Moreover, the line width which is a measure of spin wave damping also increases with increasing spin wave energy.

VI. ORBITAL ORDERING

As mentioned earlier, ARPES and XLD experiments have found the existence of ferro orbital order between the d_{xz} and d_{xz} orbitals in pnictides. This type of orbital ordering was previously proposed^{14,43–45} to explain experimentally observed in-plane anisotropic behavior like anisotropy in magnetic exchange coupling,¹⁷ transport properties,^{46,47} FS structure,⁸ and electronic structure.⁴⁸

Fig. 9 shows the band dispersion (near Γ point) in

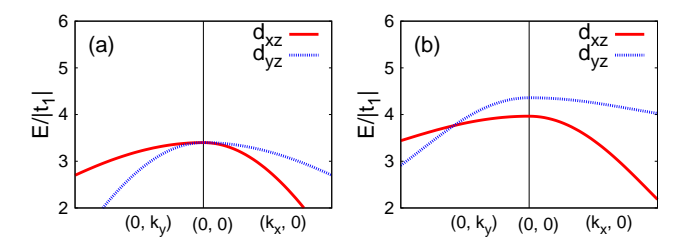


FIG. 9: Dispersion of d_{xz} and d_{yz} bands in the (a) non-magnetic state and (b) $(\pi,0)$ SDW state, showing that the d_{yz} band is pushed up in energy relative to d_{xz} band in the SDW state, resulting in ferro orbital order $(n_{xz} - n_{yz} > 0)$.

the paramagnetic and $(\pi,0)$ SDW states. While the d_{xz} and d_{uz} orbitals are degenerate in the non-magnetic state due to C_4 symmetry, the degeneracy is lifted in the SDW state and d_{yz} band is pushed up in energy relative to d_{xz} band, causing electron density difference in the two orbitals. In the $(\pi,0)$ state with exchange field parameters same as used in Fig. 7(a), electron fillings in different orbitals are obtained as $n_{xz} \approx 0.96$, $n_{yz} \approx 0.74$ and $n_{xy} \approx 0.30$. This sign of ferro-orbital order $(n_{xz} > n_{yz})$ is in agreement with experiments.^{8,11–13} As highlighted earlier, ⁴⁹ the presence of hopping anisotropy ($|t_1| > |t_2|$) along with anisotropic $(\pi,0)$ magnetic order breaks the equivalence between a and b directions, and naturally leads to orbital ordered state. Spin wave excitations in similar ferro orbital ordered state was previously carried out within a degenerate double-exchange model including antiferromagnetic superexchange interactions.⁵⁰ However, the sign of the reported $(n_{yz} > n_{xz})$ ferro orbital order does not agree with experiments. Furthermore, for a realistic NN hopping value of 200 meV, their calculated spin wave energy scale of around 30 meV is well below the nearly 200 meV energy scale measured in INS experiments.

VII. CONCLUSIONS

The minimal two-band model for iron pnictides with nearly circular electron and hole pockets shows proclivity towards $(\pi,0)$ SDW ordering due to FS nesting. However, due to cancellation of induced ferromagnetic spin couplings from electron and hole pocket contributions, the very same feature of nearly identical electron and hole pockets was shown to yield vanishing ferromagnetic spin coupling and consequently vanishing spin-wave energy at the ferromagnetic zone boundary. This being in sharp contrast to the observed maximum spin-wave energy at this wave vector in inelastic neutron scattering studies necessitated the inclusion of a third d_{xy} orbital to properly account for the experimentally observed spin dynamics in iron pnictides.

A minimal three-orbital itinerant-electron model for iron prictides involving the d_{xz} , d_{yz} , and d_{xy} Fe orbitals was therefore proposed in this paper. Our investigations

of the magnetic, electronic, and orbital properties of this model showed that the three key experimental properties — electronic band structure, magnetic excitations, and ferro orbital ordering — can be well understood within a single theoretical framework, as summarized below.

The electronic FS structure in our three-orbital model at one-third filling reproduces two key features obtained in LDA calculations and observed in ARPES experiments: two circular hole pockets around the Γ point and two elliptical electron pockets around the M point of the crystallographic Brillouin zone. The elliptical electron pockets, corresponding to quasi one dimensional motion, lead to an additional Van Hove peak in the DOS near the Fermi energy, as is indeed obtained in LDA calculations. These electron pockets are therefore also responsible for the strong F spin coupling in our model, which results in maximum spin-wave energy at the FZB wave vector $\mathbf{q} = (\pi, \pi)$ as obtained in INS experiments. The strong F spin coupling in our model also accounts for the large planar anisotropy between ab plane spin couplings as considered in phenomenological spin models.

Overall, the nature of magnetic excitations, spin-wave energy scale, anisotropic spin wave damping, and absence of particle-hole continuum as calculated in our model are in agreement with experimental results. We also explored the possibility of orbital ordering in our model due to lifting of degeneracy between the d_{xz} and d_{yz} bands and found the existence of a ferro orbital order between the d_{xz} and d_{yz} orbitals in the $(\pi,0)$ SDW state, in agreement with experiments.

Acknowledgements

Sayandip Ghosh acknowledges financial support from Council of Scientific and Industrial Research, India.

Appendix A: Spin excitations in multi-orbital model

We consider a general multi-orbital $(\pi, 0)$ ordered magnetic state involving \mathcal{N} orbitals per site, and briefly discuss spin wave excitations in this state. The transverse spin susceptibility in this spontaneously brokensymmetry state is obtained from the time-ordered propagator of the transverse spin operators $S_{i\mu}^-$ and $S_{j\nu}^+$ for sites i, j and orbitals μ, ν :

$$[\chi^{-+}(\omega)]_{i\mu;j\nu} = \int dt e^{i\omega(t-t')} \langle T_t S_{i\mu}^-(t) S_{j\nu}^+(t') \rangle, \quad (A1)$$

where T_t is the time ordering operator. As translational symmetry is preserved within the two-sublattice basis, Fourier transformation yields

$$[\chi^{-+}(\mathbf{q},\omega)]_{\alpha\beta} = \sum_{i} e^{-i\mathbf{q}\cdot(\mathbf{r}_{i}-\mathbf{r}_{j})} [\chi^{-+}(\omega)]_{i\mu;j\nu}, \quad (A2)$$

where α , β refer to indices in the composite sublatticeorbital basis, and run through $1-2\mathcal{N}$. Retaining only ladder diagrams yields the spin wave propagator in the random phase approximation (RPA):

$$\left[\chi_{\mathrm{RPA}}^{-+}(\mathbf{q},\omega)\right] = \frac{\left[\chi^{0}(\mathbf{q},\omega)\right]}{\mathbf{1} - \left[U\right]\left[\chi^{0}(\mathbf{q},\omega)\right]} \tag{A3}$$

expressed in a matrix form in the composite sublattice-orbital basis. Here, the interaction matrix [U] includes U (intra-orbital interaction) as diagonal elements and J (Hund's coupling) as off-diagonal elements. The inter-orbital density interaction and the pair hopping terms do not contribute to magnetism up to RPA level.

The bare susceptibility is calculated from the Hartree-Fock (HF) level Green's function as:

$$[\chi^{0}(\mathbf{q},\omega)]_{\alpha\beta} = i \int \frac{d\omega'}{2\pi} \sum_{\mathbf{k}} [G^{0}_{\uparrow}(\mathbf{k},\omega')]_{\alpha\beta} \times [G^{0}_{\downarrow}(\mathbf{k}-\mathbf{q},\omega'-\omega)]_{\beta\alpha} = \sum_{\mathbf{k},l,m} \left[\frac{\phi^{\alpha}_{\mathbf{k}\uparrow l}\phi^{\beta}_{\mathbf{k}\uparrow l}\phi^{\alpha}_{\mathbf{k}-\mathbf{q}\downarrow m}\phi^{\beta}_{\mathbf{k}-\mathbf{q}\downarrow m}}{E^{+}_{\mathbf{k}-\mathbf{q}\downarrow m} - E^{-}_{\mathbf{k}\uparrow l} + \omega - i\eta} \right]$$

$$+ \frac{\phi^{\alpha}_{\mathbf{k}\uparrow l}\phi^{\beta}_{\mathbf{k}\uparrow l}\phi^{\alpha}_{\mathbf{k}-\mathbf{q}\downarrow m}\phi^{\beta}_{\mathbf{k}-\mathbf{q}\downarrow m}}{E^{+}_{\mathbf{k}\uparrow l} - E^{-}_{\mathbf{k}-\mathbf{q}\downarrow m} - \omega - i\eta} \right]$$
(A4)

in the sublattice-orbital basis, and involves integrating out the fermions in the $(\pi,0)$ ordered spontaneously-broken-symmetry state. Here $E_{\mathbf{k}\sigma}$ and $\phi_{\mathbf{k}\sigma}$ are the eigenvalues and eigenvectors of the HF level Hamiltonian matrix and l,m indicate the eigenvalue branches. The superscripts +(-) refer to particle (hole) energies above (below) the Fermi energy, and both inter-band and intraband particle-hole terms are included. The spin wave energies are obtained from the poles of Eqn. A3.

Appendix B: Hartree-Fock approximation

Here, we discuss the Hartree-Fock (mean field) treatment of the onsite interaction terms given in Eq. 3. The

mean-field parameters n_{μ} and m_{μ} describe the charge density and sublattice magnetization of the orbital μ , and the rest of the notation is standard. The intra-orbital Coulomb interaction term in this approximation is given by:

$$H_{\rm HF}^{\rm intra} = \frac{U}{2} \sum_{\mathbf{k},\mu,\sigma} \left(-\sigma \tau m_{\mu} + n_{\mu} \right) a_{\mathbf{k},\mu,\sigma}^{\dagger} a_{\mathbf{k},\mu,\sigma} a_{\mathbf{k},\mu,\sigma} + \text{const},$$
(B1)

where $\tau = +(-)$ for sublattice A(B) in which $\uparrow (\downarrow)$ spins are majority. The inter-orbital Coulomb interaction and and the Hund's coupling terms take the forms:

$$H_{\rm HF}^{\rm inter} = (U' - \frac{J}{2}) \sum_{\mathbf{k}, \mu \neq \nu, \sigma} n_{\nu} a_{\mathbf{k}, \mu, \sigma}^{\dagger} a_{\mathbf{k}, \mu, \sigma} + \text{const},$$
 (B2)

and

$$H_{\rm HF}^{\rm Hunds} = -\frac{J}{2} \sum_{\mathbf{k}, \mu \neq \nu, \sigma} \sigma \tau m_{\nu} a_{\mathbf{k}, \mu, \sigma}^{\dagger} a_{\mathbf{k}, \mu, \sigma} + \text{const}$$
 (B3)

respectively. The pair-hopping term does not contribute to the mean-field level Hamiltonian.

The total interaction Hamiltonian decouples into magnetic and density terms:

$$H_{\rm HF}^{I} = -\sigma\tau \sum_{\mathbf{k},\mu,\sigma} \Delta_{\mu} a_{\mathbf{k},\mu,\sigma}^{\dagger} a_{\mathbf{k},\mu,\sigma}$$

$$+ \frac{5J - U}{2} \sum_{\mathbf{k},\mu,\sigma} n_{\mu} a_{\mathbf{k},\mu,\sigma}^{\dagger} a_{\mathbf{k},\mu,\sigma} + \text{const}, (B4)$$

with the self-consistent exchange fields defined as $2\Delta_{\mu} = U m_{\mu} + J \sum_{\nu \neq \mu} m_{\nu}$. Here, we have taken a constant total electron filling $(\sum_{\mu} n_{\mu})$ and U' = U - 2J.

^{*} Electronic address: sayandip@iitk.ac.in, sayandip.cmt@gmail.comHe, M. Hashimoto, R. G. Moore, I. I. Mazin, D. J. Singh,

J. Zhao, Q. Huang, C. de la Cruz, S. Li, J. W. Lynn, Y. Chen, M. A. Green, G. F. Chen, G. Li, Z. Li, J. L. Luo, N. L. Wang, and P. Dai, Nature Mat. 7, 953 (2008).

² S. Nandi, M. G. Kim, A. Kreyssig, R. M. Fernandes, D. K. Pratt, A. Thaler, N. Ni, S. L. Bud'ko, P. C. Canfield, J. Schmalian, R. J. McQueeney, and A. I. Goldman, Phys. Rev. Lett. **104**, 057006 (2010).

³ K. Haule, J. H. Shim, and G. Kotliar, Phys. Rev. Lett. 100, 226402 (2008).

⁴ D. J. Singh, and M.-H. Du, Phys. Rev. Lett. **100**, 237003 (2008).

⁵ I. A. Nekrasov, Z. V. Pchelkina, and M. V. Sadovskii, JETP letters 88, 144 (2008).

⁶ M. Yi, D. H. Lu, J. G. Analytis, J.-H. Chu, S.-K. Mo, R.-H.

Z. Hussain, I. R. Fisher, and Z.-X. Shen, Phys. Rev. B 80, 174510 (2009).

⁷ T. Kondo, R. M. Fernandes, R. Khasanov, Chang Liu, A. D. Palczewski, Ni Ni, M. Shi, A. Bostwick, E. Rotenberg, J. Schmalian, S. L. Bud'ko, P. C. Canfield, and A. Kaminski, Phys. Rev. B 81, 060507(R) (2010).

⁸ M. Yi, D. Lu, J.-H. Chu, J. G. Analytis, A. P. Sorini, A. F. Kemper, B. Moritz, S.-K. Mo, R. G.Moore, M. Hashimoto, W.-S. Lee, Z. Hussain, T. P. Devereaux, I. R. Fisher, and Z-X Shen, Proc. Nat. Acad. Science 108, 6878 (2011).

⁹ V. Brouet, M. F. Jensen, P.-H. Lin, A. Taleb-Ibrahimi, P. Le Fèvre, F. Bertran, C.-H. Lin, Wei Ku, A. Forget, and D. Colson, Phys. Rev. B 86, 075123 (2012).

¹⁰ A. A. Kordyuk, V. B. Zabolotnyy, D. V. Evtushinsky, A. N.

- Yaresko, B. Büchner, and S. V. Borisenko, J. Supercond. Nov. Magn. **26**, 2837 (2013).
- ¹¹ T. Shimojima, K. Ishizaka, Y. Ishida, N. Katayama, K. Ohgushi, T. Kiss, M. Okawa, T. Togashi, X-Y Wang, C-T Chen, S. Watanabe, R. Kadota, T. Oguchi, A. Chainani, and S. Shin, Phys. Rev. Lett. **104**, 057002 (2010).
- M. F. Jensen, V. Brouet, E. Papalazarou, A. Nicolaou, A. Taleb-Ibrahimi, P. Le Fèvre, F. Bertran, A. Forget, and D. Colson, Phys. Rev. B 84, 014509 (2011).
- Y. K. Kim, W. S. Jung, G. R. Han, K.-Y. Choi, K.-H. Kim, C.-C. Chen, T. P. Devereaux, A. Chainani, J. Miyawaki, Y. Takata, Y. Tanaka, M. Oura, S. Shin, A. P. Singh, H. G. Lee, J.-Y. Kim, and C. Kim, Phys. Rev. Lett. 111, 217001 (2013).
- ¹⁴ W. Lv, J. Wu, and Philip Phillips, Phys. Rev. B **80**, 224506 (2009).
- J. Zhao, D.-X. Yao, S. Li, T. Hong, Y. Chen, S. Chang, W. Ratcliff II, J. W. Lynn, H. A. Mook, G. F. Chen, J. L. Luo, N. L. Wang, E. W. Carlson, Jiangping Hu, and P. Dai, Phys. Rev. Lett. 101, 167203 (2008).
- ¹⁶ R. A. Ewings, T. G. Perring, R. I. Bewley, T. Guidi, M. J. Pitcher, D. R. Parker, S. J. Clarke, and A. T. Boothroyd, Phys. Rev. B 78, 220501(R) (2008).
- ¹⁷ J. Zhao, D. T. Adroja, Dao-Xin Yao, R. Bewley, S. Li, X. F. Wang, G. Wu, X. H. Chen, J. Hu, and P. Dai, Nature Physics 5, 555 (2009).
- ¹⁸ S. O. Diallo, V. P. Antropov, T. G. Perring, C. Broholm, J. J. Pulikkotil, N. Ni, S. L. Bud'ko, P. C. Canfield, A. Kreyssig, A. I. Goldman, and R. J. McQueeney, Phys. Rev. Lett. **102**, 187206 (2009).
- ¹⁹ R. A. Ewings, T. G. Perring, J. Gillett, S. D. Das, S. E. Sebastian, A. E. Taylor, T. Guidi, and A. T. Boothroyd, Phys. Rev. B 83, 214519 (2011).
- ²⁰ L. W. Harriger, H. Q. Luo, M. S. Liu, C. Frost, J. P. Hu, M. R. Norman, and P. Dai, Phys. Rev. B 84, 054544 (2011).
- ²¹ N. Raghuvanshi, and A. Singh, J. Physics: Condens. Matter, **22**, 422202 (2010).
- ²² S. Raghu, X.-L. Qi, C.-X. Liu, D. J. Scalapino, and S.-C. Zhang, Phys. Rev. B **77**, 220503(R) (2008).
- ²³ Q. Han, Y. Chen, and Z. D. Wang, Europhys. Lett. 82, 37007 (2008).
- ²⁴ M. Daghofer, A. Moreo, J. A. Riera, E. Arrigoni, D. J. Scalapino, and E. Dagotto, Phys. Rev. Lett. **101**, 237004 (2008).
- N. Raghuvanshi, and A. Singh, J. Physics: Condens. Matter, 23, 312201 (2011).
- ²⁶ J. Knolle, I. Eremin, and R. Moessner, Phys. Rev. B 83, 224503 (2011).
- ²⁷ Patrick A. Lee and Xiao-Gang Wen, Phys. Rev. B 78, 144517 (2008).
- ²⁸ M. Daghofer, A. Nicholson, A. Moreo, and E. Dagotto,

- Phys. Rev. B 81, 014511 (2008).
- ²⁹ Sen Zhou, and Ziqiang Wang, Phys. Rev. Lett. **105**, 096401 (2010).
- ³⁰ R. Yu, K. T. Trinh, A. Moreo, M. Daghofer, J. A. Riera, S. Haas, and E. Dagotto, Phys. Rev. B **79**, 104510 (2009).
- ³¹ S Graser, T A Maier, P J Hirschfeld, and D J Scalapino, New J. Phys. 11, 025016 (2009).
- ³² Hiroaki Ikeda, Ryotaro Arita, and Jan Kuneš, Phys. Rev. B 81, 054502 (2010).
- ³³ S. Graser, A. F. Kemper, T. A. Maier, H.-P. Cheng, P. J. Hirschfeld, and D. J. Scalapino, Phys. Rev. B 81, 214503 (2010).
- ³⁴ E. Kaneshita, and T. Tohyama, Phys. Rev. B **82**, 094441 (2010).
- ³⁵ K. Kuroki, S. Onari, R. Arita, H. Usui, Y. Tanaka, H. Kontani, and Hideo Aoki, Phys. Rev. Lett. **101**, 087004 (2008).
- ³⁶ A. Singh, arXiv:cond-mat/0112442 (2001).
- ³⁷ P M R Brydon, Maria Daghofer, and Carsten Timm, J. Physics: Condens. Matter, 23, 246001 (2011).
- ³⁸ I. I. Mazin, D. J. Singh, M. D. Johannes, and M. H. Du, Phys. Rev. Lett. **101**, 057003 (2008).
- ³⁹ Helmut Eschrig, and Klaus Koepernik, Phys. Rev. B 80, 104503 (2009).
- ⁴⁰ Q. Luo, G. Martins, D.-X. Yao, M. Daghofer, Rong Yu, A. Moreo, and E. Dagotto, Phys. Rev. B 82, 104508 (2010).
- ⁴¹ Dao-Xin Yao, and E. W. Carlson, Phys. Rev. B **78**, 052507 (2008).
- ⁴² J. Knolle, I. Eremin, A. V. Chubukov, and R. Moessner, Phys. Rev. B **81**, 140506(R) (2010).
- ⁴³ C.-C. Lee, W.-G. Yin, and W. Ku, Phys. Rev. Lett. **103**, 267001 (2009).
- ⁴⁴ C.-C. Chen, J. Maciejko, A. P. Sorini, B. Moritz, R. R. P. Singh, and T. P. Devereaux, Phys. Rev. B 82, 100504(R) (2010)
- ⁴⁵ W. Lv, and P. Phillips, Phys. Rev. B **84** 174512 (2011).
- M. A. Tanatar, E. C. Blomberg, A. Kreyssig, M. G. Kim, N. Ni, A. Thaler, S. L. Bud'ko, P. C. Canfield, A. I. Goldman, I. I. Mazin, and R. Prozorov, Phys. Rev. B 81, 184508 (2010).
- ⁴⁷ J-H Chu, J. G. Analytis, K. De Greve, P. L. McMahon, Z. Islam, Y. Yamamoto, I. R. Fisher, Science 329, 824 (2010).
- ⁴⁸ T-M Chuang, M. P. Allan, J. Lee, Xie Yang, Ni Ni, S. L. Bud'ko, G. S. Boebinger, P. C. Canfield, and J. C. Davis, Science 327, 181 (2010).
- ⁴⁹ Sayandip Ghosh, and Avinash Singh, Journal of Applied Physics 115, 103907 (2014).
- ⁵⁰ W. Lv, F. Krüger, and P. Phillips, Phys. Rev. B 82, 045125 (2010).